Performance testing of a podded propeller in the cavitation tunnel

Kavanagh, B.

Publisher's version / Version de l'éditeur:
https://doi.org/10.4224/8894988
Laboratory Memorandum; no. LM-2004-12, 2004

National Research Council Canada
Conseil national de recherches Canada
Institute for Ocean Technology
Institut des technologies océaniques

Laboratory Memorandum

LM-2004-12

Performance Testing of a Podded Propeller in the Cavitation Tunnel

B. Kavanaugh

April 2004

Canada

DOCUMENTATION PAGE

REPORT NUMBER	NRC REPORT NUMBER	DATE
LM-2004-12		April 2004
REPORT SECURITY CLASSIFICATION		**DISTRIBUTION**
Unclassified		Unlimited

TITLE

PERFORMANCE TESTING OF A PODDED PROPELLER IN THE CAVITATION TUNNEL

AUTHOR(S)

Brent Kavanagh

CORPORATE AUTHOR(S)/PERFORMING AGENCY(S)

Institute for Ocean Technology, National Research Council, St. John's, NL

PUBLICATION

SPONSORING AGENCY(S)

Institute for Ocean Technology, National Research Council, St. John's, NL

IMD PROJECT NUMBER	NRC FILE NUMBER		
KEY WORDS	**PAGES**	**FIGS.**	**TABLES**
Foxboro, Propeller Hub Geometry, Cavitation	24	4	4

SUMMARY

This study presents the results of testing carried out on a model propeller developed and manufactured as part of a partnership between the Institute for Ocean Technology, Memorial Univeristy and industrial partners Oceanic Consulting and Thordon Bearings. Testing was conducted to investigate the performance and cavitation characteristics of a propeller with a given propeller hub geometry, and it will be compared with future tests to develop a fuller understanding of the effects of propeller-hub geometry on performance characteristics.

ADDRESS National Research Council
Institute for Ocean Technology
Arctic Avenue, P. O. Box 12093
St. John's, NL A1B 3T5
Tel.: (709) 772-5185, Fax: (709) 772-2462

National Research Council Canada
Institute for Ocean Technology

Conseil national de recherches Canada
Institut des technologies océaniques

PERFORMANCE TESTING OF A PODDED PROPELLER IN THE CAVITATION TUNNEL

LM-2004-12

Brent Kavanagh

April 2004

ABSTRACT
This study presents the results of testing carried out on a model propeller developed and manufactured as part of a partnership between the Institute for Ocean Technology, Memorial University and industrial partners Oceanic Consulting and Thordon Bearings. Testing was conducted to investigate the performance and cavitation characteristics of a propeller with a given propeller hub geometry, and it will be compared with future tests to develop a fuller understanding of the effects of propeller-hub geometry on performance characteristics. This is all being carried out as part of the work of Rocky Taylor, towards his masters in engineering at Memorial University of Newfoundland.

TABLE OF CONTENTS

LIST OF TABLES

LIST OF FIGURES

1.0 INTRODUCTION

Podded propellers were introduced to the marine industry a little over a decade ago, and have since found application in a variety of roles. A podded propeller consists of an electric drive motor inside a pod, with a propeller(s) connected by a drive shaft at one or both ends of the pod. This pod is connected to the hull of the ship via a strut and slewing bearing assembly that allows the entire unit to rotate. This allows the thrust developed by the propeller to be directed anywhere in a 360 degree compass, and eliminates the need for a rudder, while providing far superior maneuvering capabilities for a vessel. However, this rapid acceptance by the industry has outpaced the understanding of their performance, and thus created a need for research into their design and operation.

There have been studies into the performance, cavitation and accompanying noise characteristics of podded propellers (M. Atlar et al., 2001), but thus far limited research has been done into the effect of the pod shape on these performance parameters. This study is intended to investigate the effects of the hub geometry on the cavitation characteristics and performance of propellers designed for use with pods. By attaining a better understanding it is possible to improve the overall design of the pod to yield better performance from the propeller. A conscious effort was taken not to use a specific final application in mind in this study, and as such the geometries were chosen to keep the results of more general use. All testing was done in the cavitation tunnel at the National Research Council Institute for Ocean Technology. The propeller was tested at various cavitation numbers (σ values) and various advance coefficients (J Values).

2.0 METHOD

The required conditions for each of the variables were obtained by changing the absolute tunnel pressure, and the water flow rate as dictated by the following formulae.

$$J = \frac{V_A}{nD} \tag{1}$$

$$\sigma = \frac{\rho g h + P_{tunnel\_abs} - P_{Vap}}{0.5 \rho n^2 D^2} \tag{2}$$

Where V_A is the flow rate of the water (in *m/s*), n is the rotational speed (in *revolution per second*), D is the diameter of the propeller (in *m*), ρ is density of the water (in kg/m^3), g is the gravitational constant (9.81 m/s^2), *h* is the shaft depth (in *m*), P_{tunnel_abs} is the absolute pressure inside the tunnel and P_{Vap} is the saturated vapor pressure, (both measured in N/m^2). P_{Vap} is a function of the water temperature, and in this test was equal to 16°C. All tests were conducted using a Reynolds Number of 4.02×10^6, in accordance with the ITTC criteria of testing propeller in a tunnel at the highest cavitation numbers possible.

The cavitation tunnel at the Institute for Ocean Technology has been described in detail in previous documentation (Doucet, 1992), however the details of the tunnel have been summarized below. A schematic of the tunnel has been attached in Appendix A.

Table 2.1: Tunnel Specifications

Test Section Dimensions	0.5m x 0.5m x 2.2m
Water Speeds	0 – 10.0 m/s
Propeller Speeds	0 – 1800 rpm or 30 rps
Test Section Pressures	10 kPa to 200 kPa (absolute)

The tunnel is equipped with Foxboro software, a computer control system that allows for precise control of all propeller, flow, pressure and filtration conditions. All torque and thrust measurements were made using a sealed strain gauge dynamometer mounted between the propeller and first shaft bearing with a ± 900 N thrust range and ± 45Nm torque range. All pressure and flow measurements were made using differential pressure transducers, and the rotational speed of the propeller was measured using a digital tachometer. And as well an oxygen sensor is used to give the gas content measurements to ensure proper cavitation scaling.

2.1 PROPELLER DESIGN AND MANUFACTURE

The propeller used in the testing borrowed the basis of its geometry from two real podded propellers found on two tankers, (P. Liu, Unpublished). The base geometry is similar to the P4119 and is named PP00+00C0. The geometric specifications can be seen in the following table.

Table 2.2: Basic Propeller Model Geometry

Pitch Ratio at 0.7R	1.0
Rake	0.0°
Skew	0.0°
Direction of Rotation	Right Hand
Radius	270mm
Number of Blades	4

The propeller name is merely a summary of the key points in this table, and can be explained as explained as P for podded, P for Propeller, 00 for zero skew, +00 for zero positive rake, C/V for constant or a variable pitch and 0/1/... for the NACA 66 modified/critical cavitation number based/etc. It is also important to note that while the propeller diameter of 0.27m exceeds the maximum recommended of diameter of 0.25 m, there were minimal wall effects as will be demonstrated later in later sections.

2.2 PROPELLER BLADE SECTION GEOMETRY

The propeller blade section is a version of the NACA 66 (DTMB modified) foil, using a A=0.8 meanline. The sectional geometry offsets are then included in the chart below. C_d is the normalized chord length, P_d is the pitch ratio, and T_c and F_c represent the maximum thickness and maximum camber respectively all for the respective radial position.

Table 2.3: Sectional Geometry Offsets for PP00+0C0

Radius (%)	C_d	P_d	T_c	F_c
0.20	0.252072	1.1050	0.20550	0.01429
0.30	0.28555	1.1020	0.15530	0.02318
0.40	0.318871	1.0980	0.11800	0.02303
0.50	0.345968	1.0930	0.09160	0.02182
0.60	0.363141	1.0880	0.06960	0.02072
0.70	0.364086	1.0840	0.05418	0.02003
0.80	0.342424	1.0810	0.04206	0.01967
0.90	0.284605	1.0790	0.03321	0.01817
0.95	0.218593	1.0770	0.03228	0.01631
1.00	0.00	1.0750	0.03160	0.01175

The normalized cross sectional geometry is given in the following chart. All blade cross sections will have the same shape, although obviously they will be of differing size. T/C is the percentage of the maximum thickness at a given position, and F/C is a percentage of the maximum camber at a given position. X/C is the chord position normalized by the chord length. A cross sectional outline for the radial position of 0.3 R has also been included, and is shown in Figure 1.

Table 2.4: Thickness and Camber Distribution for PP00+0C0

X/C	T/C	F/C
0.000	0.000	0.000
0.0125	0.2088	0.0907
0.0250	0.2932	0.1586
0.0500	0.4132	0.2712
0.0750	0.5050	0.3657
0.1000	0.5814	0.4482
0.1500	0.7042	0.5869
0.2000	0.8000	0.6993
0.3000	0.9274	0.8635
0.4000	0.9904	0.9615
0.4500	1.000	0.9881
0.5000	0.9924	1.000
0.6000	0.9306	0.9786
0.7000	0.8070	0.8892
0.8000	0.6220	0.7027
0.9000	0.3754	0.3586
0.9500	0.2286	0.1713
1.000	0.0666	0.000

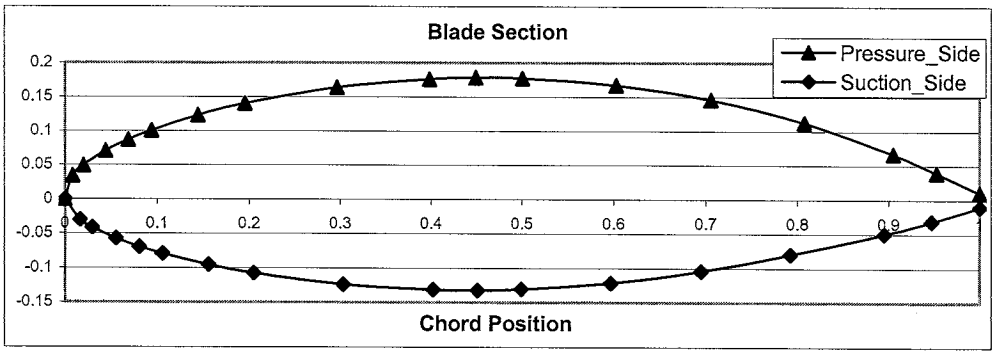

Figure 2.1: Blade Section

This plot was obtained by plotting the perpendicular off set method (Abbot and Von Doenhoff, 1949). The following formulae were employed.

$$X_u = x - y_t \sin\theta; Y_u = y_c + y_t \cos\theta \quad (3)$$

$$X_l = x + y_t \sin\theta; Y_l = y_c - y_t \cos\theta \quad (4)$$

$$\theta = \tan^{-1} \frac{\partial y_c}{\partial x_c} \quad (5)$$

Where X_u and Y_u are the coordinates of the top surface of the section and X_l and Y_l and represent coordinates of the lower surface of the section. x represents the chord position of the camber line, y_c represents the ordinate of the camber line, and y_t the ordinate of the thickness line.

The manufacturing of the model propeller was completed at Memorial University St. John's Campus, using a CNC (computer numerical control) vertical machining center. The propeller geometry was input into the PROPELLA code, which in addition to providing numerical simulation of the model, output a *.dxf propeller geometry file which was then modified and used by the CNC machining center directly to manufacture the propeller. The manufacturing tolerance for the CNC machining center is ± 0.0001m.

2.3 HUB GEOMETRY

The hub used in this test was also manufactured at Memorial University, and its geometry was of equal importance as the propeller geometry. The geometry contained within the propeller hub, is contained in the following table

Table 2.5: Basic Hub Geometry

Hub Taper Angle	20° (Upstream has larger Diameter)
Hub Diameter (d)	0.0702m
Hub Ratio (d/D)	0.26

This combination of propeller and hub geometry is actually one of a series of geometries that are to be completed before the conclusion of this project. This

combination represents the first in the series to be completed. The 3 – D graphical model is show below in Figure 2. These models were obtained through the use of the PROPELLA code, with the output *.DXF files converted to a compatible format using AutoCAD 2000.

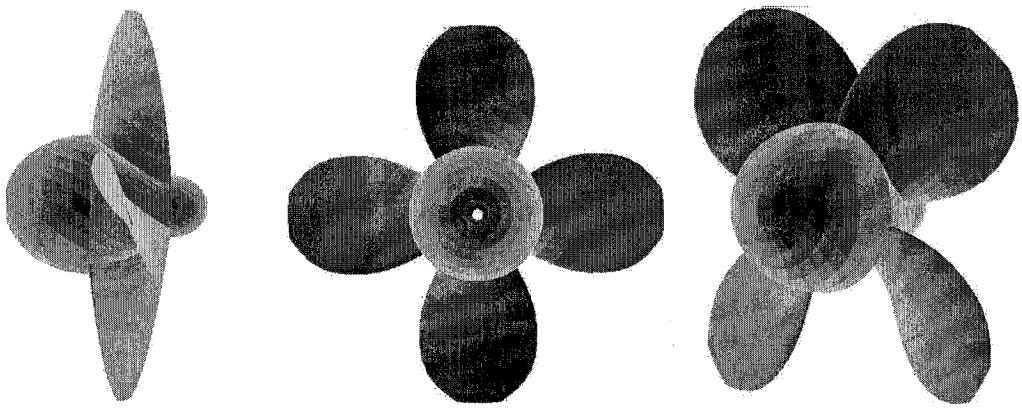

Figure 2.2: 3 - D representations of the Propeller Hub geometry

3.0 RESULTS AND DISCUSSION

Data presented in figure 3, shows the performance graphs (Kt, Kq and η) of both the open water test performed in the towing tank here at the Institute for Ocean Technology, and the cavitation tunnel test performed with a σ value equal to σ_{atm}. The close correlation between the two demonstrates a minimal wall effect in the cavitation tunnel across the entire range of J values tested. This can often be one of the largest obstacles in these types of tests. Combined plots of Kt, Kq and efficiency for each separate cavitation number are given at the end of this section, as well; graphs of the Kt, Kq and efficiency plotted vs. J are included at the end of this section.

It should also be noted that the tests were conducted for σ values ranging from 1.6 to 13.25. And while this is a wide range of cavitation constants, it does omit the most critical range from 0.5 to 1.5, which is where the most extreme

behavior can often be found. This was because the cavitation tunnel could not achieve the conditions necessary for these values. The flow rate of the water needed to be significantly slower than the advance speed of the propeller, however the propeller would effectively suck the water through and increase the flow rate of the water, and consequently increase the J value as well. This severely limited the final observations that can be drawn from these tests.

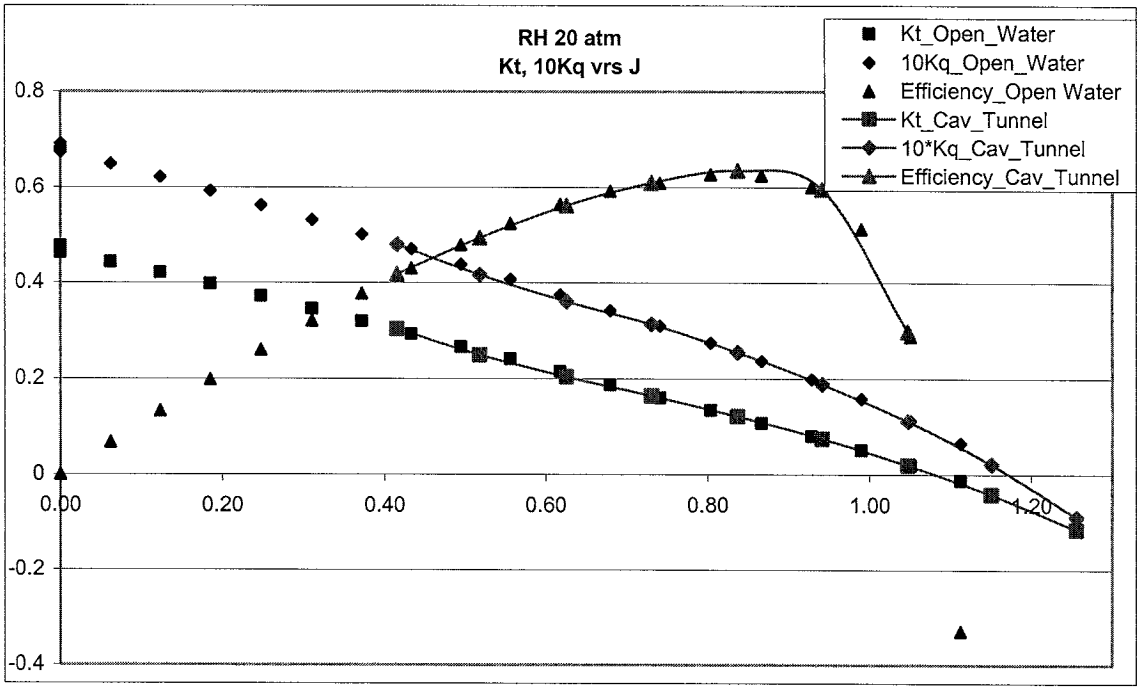

Figure 2.3: Performance curves for Towing Tank and Cavitation Tunnel at Sigma Atm

3.1 PERFORMANCE

3.1.1 Kt Curves

The results of the performance testing can be seen graphically on the following pages. The thrust coefficient data shows that as sigma increases, there is really a minimal change in the Kt values for a given advance ratio. From a starting point of σ = 1.6, the Kt increased until σ = 2.2, where it began to decrease again until σ = 4.27. From 4.27 it increases to 6.24, and from 6.24

onward, it stays relatively constant with a slight tendency to decrease with increasing σ. This abnormal behavior seems to be point anomaly, and was witnessed in the 10*Kq plot, and to a lesser extent in the efficiency curve as well. However, the other general trends were true for all J values up to J = 1. For all J greater than one, there was a portion of the σ Vs. Kt graph with crossed the x – axis and took on a negative value. For J > 1.0569, these graphs were completely negative. This indicates the water speed was faster than the advance speed of the propeller, and therefore is of no practical use.

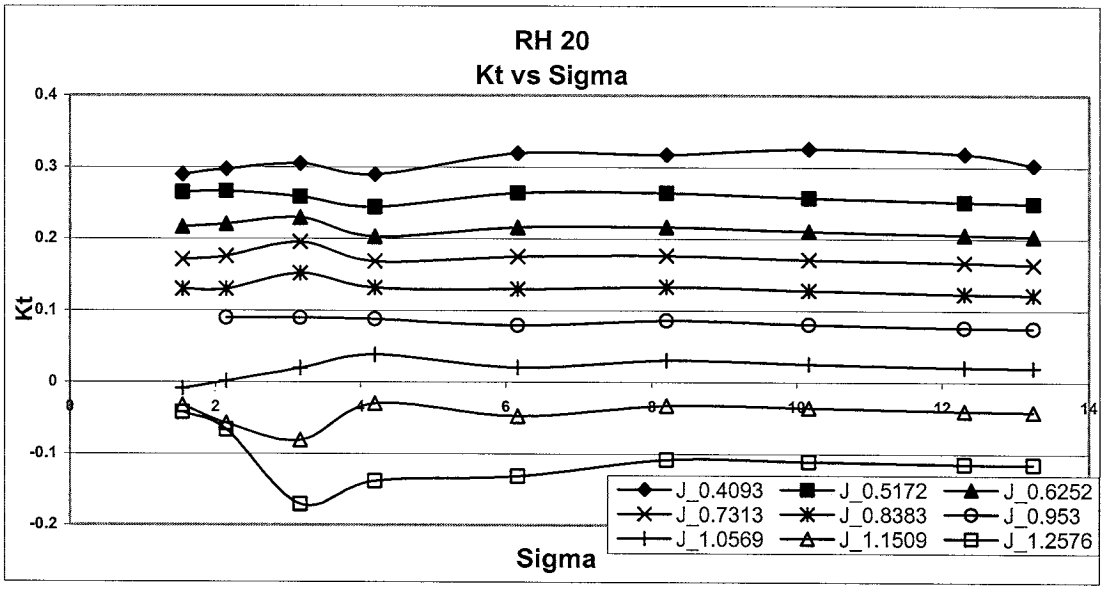

Figure 3.1: Kt Vs Sigma plot for all J

When analyzed using a constant σ, and considering it from a variable J value, it can be seen that for any constant σ value, there is a steep negative slope on the J vs. Kt curves. This is to be expected from the Kt vs. σ curves previously presented. However, from these graphs, we can see that the slope on the Kt curve is larger for the higher σ values. We can also see here that the Kt curves take on negative values when J is approximately 1.1, for all σ. This gives a more accurate representation of the operating range than the Kt vs. σ plots. There was

also more variation among the 10*Kq plots for varied σ than was seen in the Kt plots. This indicates more fluctuation in the shaft torque than would be seen in the thrust generated.

3.1.2 Kq Curves

As was expected, many of the same tendencies displayed by the Kt curves were displayed by the Kq curves. The 10*Kq Vs σ plots displayed the same fluctuations for around σ = 4.27, however where the Kt curves tended to decrease slightly with increasing σ, the 10*Kq curves tend to increase slightly. This indicates that as the σ values increase, so too does the load in the propeller shaft. This is not a desirable tendency especially when combined with the previously mentioned trend toward decreasing thrust with increasing σ. We also see again negative values for 10*Kq once J exceeds 1.05, although it does not go negative for all sigma until J = 1.2576. This is a higher J threshold than we saw in the Kt plots. And while it is interesting to note, it does not give much practical information.

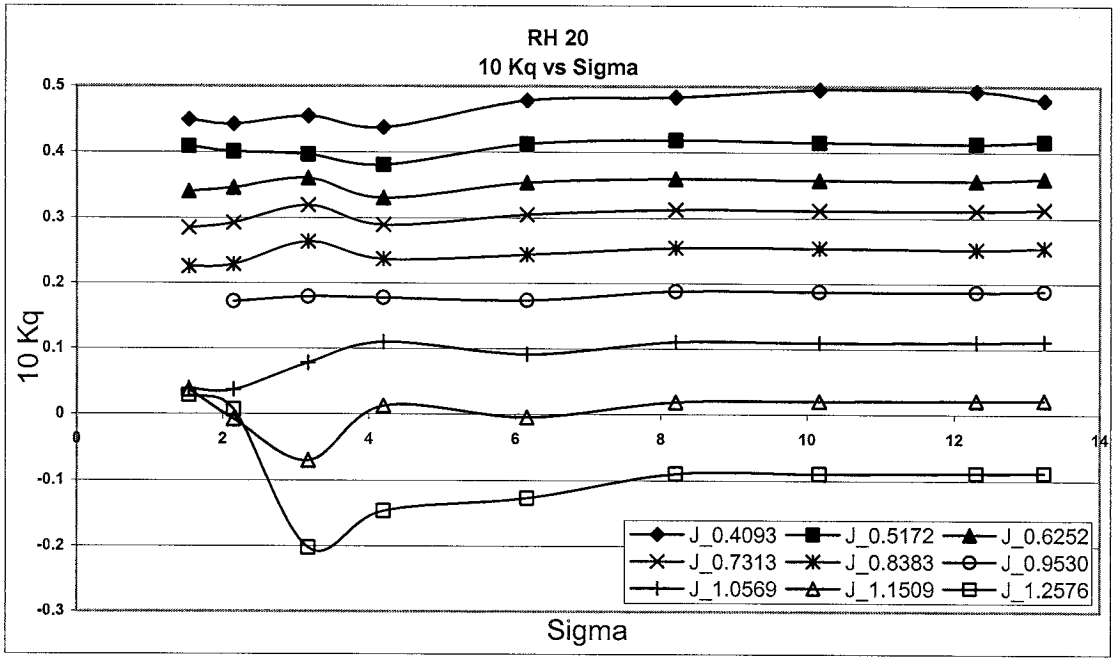

Figure 3.2: 10*Kq Vs Sigma Plot for all J

From the 10*Kq Vs J graphs, we can again see the same general tendencies as with the Kt plots. The biggest difference being that the 10*Kq plots stayed positive until higher J values were used for any corresponding σ.

3.1.3 Efficiency Curves

The efficiency Vs σ curves demonstrate two clear tendencies. The first is a tendency toward decreasing η with an increasing σ. All curves have a similar slope, with the exception of J = 0.9530, which has a much steeper slope than any of the others. It should also be noted that we omitted the η curves for all J > 1.00 because the negative nature of the Kt and Kq curves, led to unrealistic η curves. The second trend noticed was the tendency toward increasing efficiency with increasing J. Again the exception to this trend was J = 0.9530, which attained the highest overall efficiency when σ = 2.22, but dropped more dramatically as σ increased.

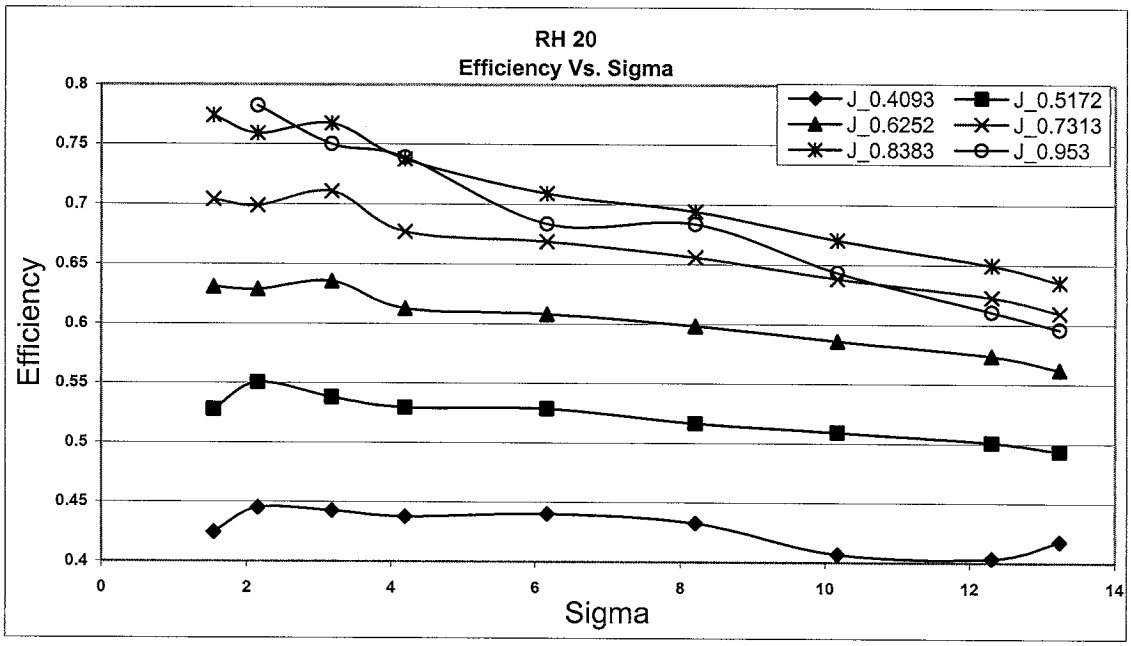

Figure 3.3: Efficiency Vs. Sigma Plot for all J

The η Vs. J curves all displayed similar trends, with an almost linear increase in efficiency with increasing J until a peak efficiency was reached within the range of J =0.85 to 0.95, depending on the corresponding σ, and then dropped sharply off. It was also noticed that at lower sigma values, the curves had smaller slopes, indicating less dependency on J, and thus a more predicable performance over a wide range of J values.

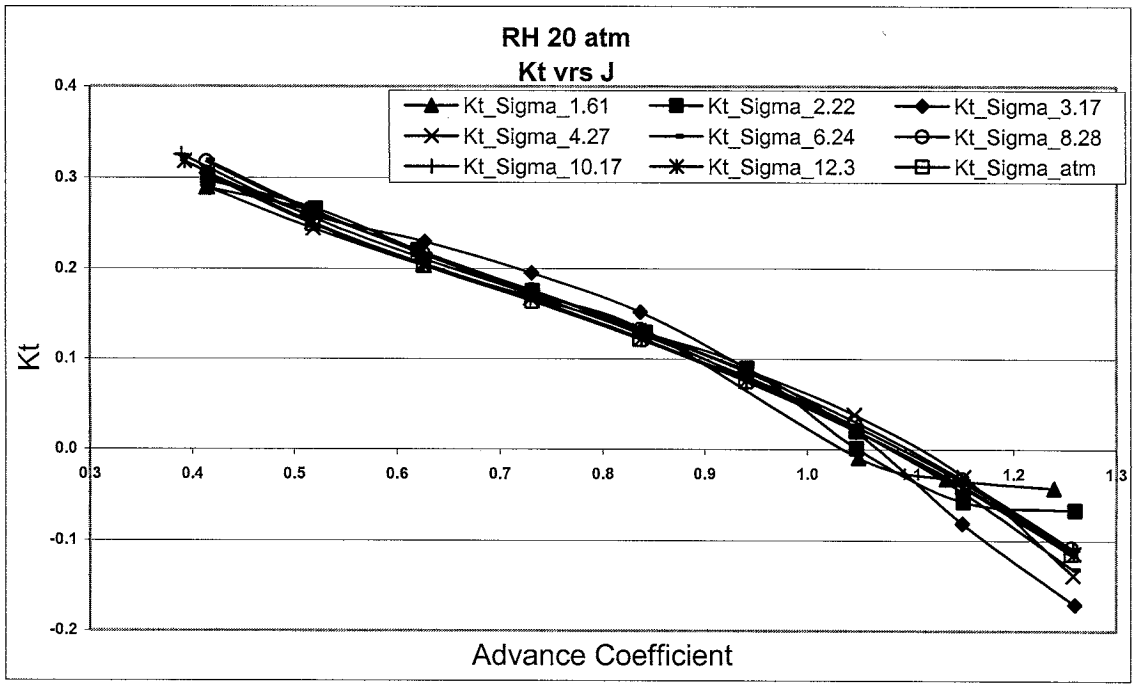

Figure 3.4: Plot of Thrust Coefficient Vs Advance Coefficient for Varied Sigma

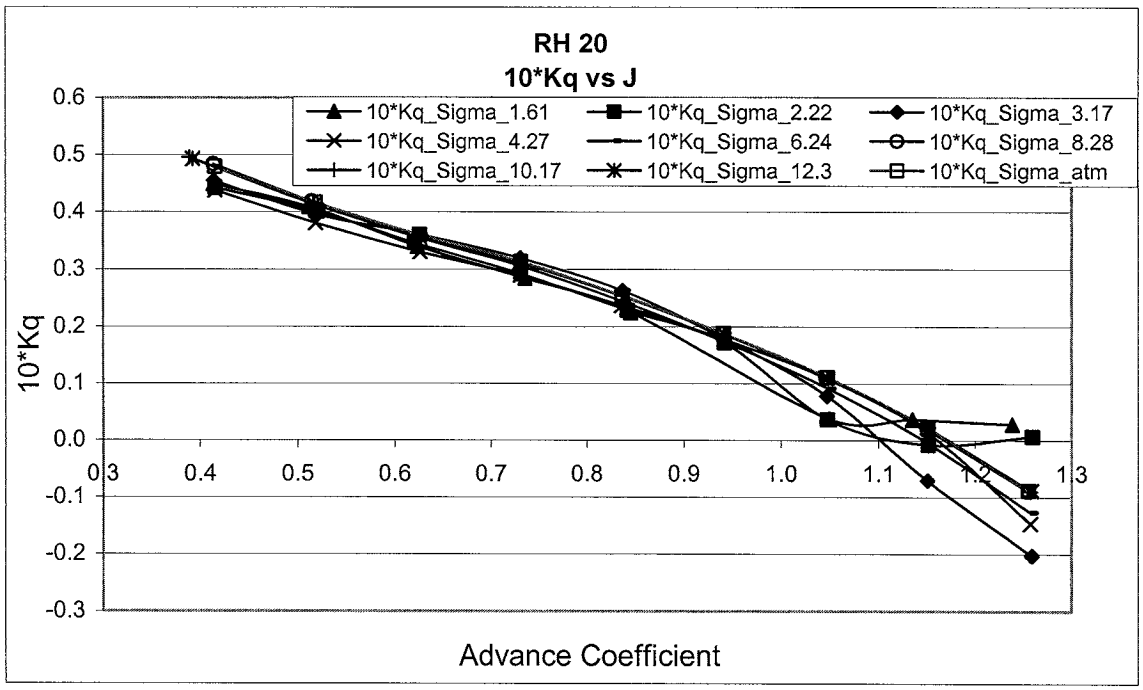

Figure 3.5: Plot of Torque Coefficient Vs Advance Coefficient for Varied Sigma

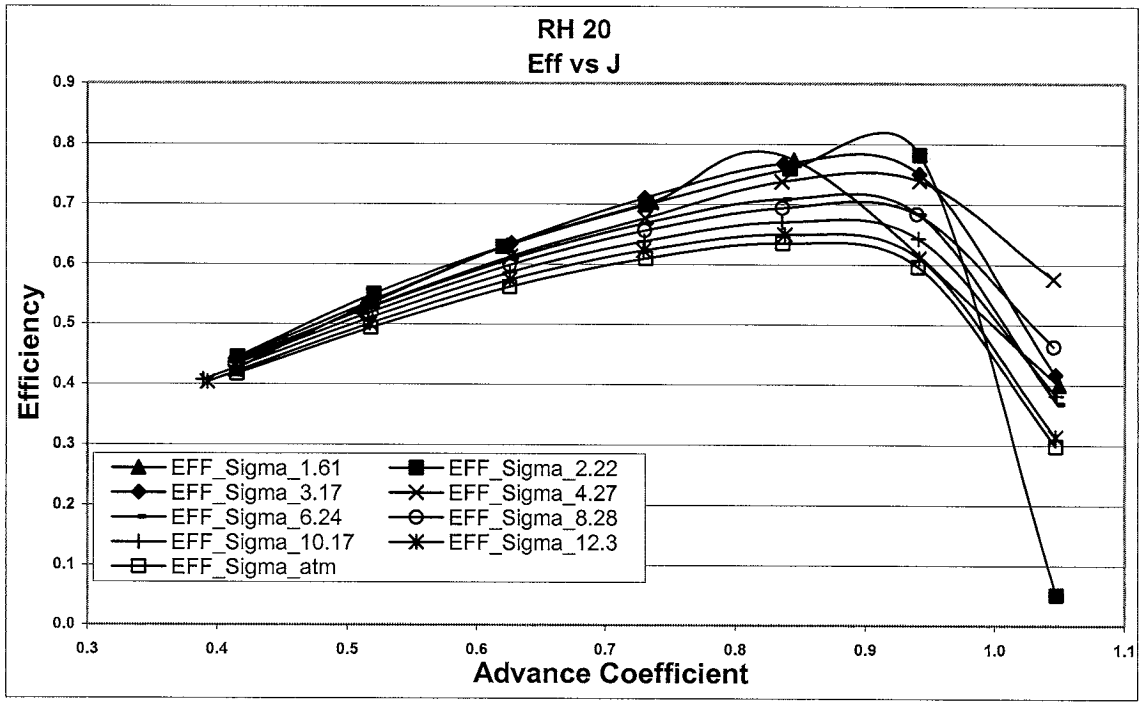

Figure 3.6: Plot of Efficiency Vs Advance Coefficient for Varied Sigma

3.2 CAVITATION

The analysis of the cavitation conditions is best analyzed on a case-by-case basis, and the general trends drawn once all the information has been presented. The testing was carried out for across a range of advance ratios, at a number of different σ values. These σ values were held constant for each individual set of J values. It should also be noted that cavitation inception was taken to be the point at which cavitation was witnessed on all blades, at least once for any two second interval chosen from the test footage. The test footage was obtained using a MiniDV digital video camera capturing at 30 frames-per-second, and stroboscopic lighting for 4 of the 8 test conditions. Footage was obtained for σ = 2.22, 4.27, 6.24 and 8.28. However, the cavitation data is not as detailed as would be liked, because the footage obtained for three of the four trials, was take from the pressure side of the propeller and thus yields little practical cavitation data. This is not in accordance with ITTC standards (ITTC, 2002). ITTC standards require footage be taken from *both* the pressure side and the suction side to give the fullest possible picture of the cavitation patterns. Another non-standard approach taken in this test is the lack of radial position markings on the propeller blade. ITTC standard test would normally have constant radius lines marked on the propeller, typically at 0.5, 0.7 and 0.9 radius. This is to allow more accurate description of the location of cavitation on the propeller blade, that being said, there is still much which can be learned from these tests.

The Value of cavitation number σ = 2.22 was the lowest tested of the σ values, and also the value for which we did attain footage of the suction side. Tip vortex cavitation was first noticed at an advance ratio of 0.7314. Once the advance ratio was lowered beyond this point, the tip vortex intensified and the vortex thickened. Also sheet cavitation was noticed on the blade at J values below 0.6205. As with the vortex cavitation, the sheet cavitation also intensified with decreasing J, expanding to cover more of the blade surface right up to the

lowest test J value of 0.5205. For any J values above 0.8420, there was no cavitation induced by the propeller. The cavitation patterns for the suction side can be seen Figure 8, and pictures taken from the test footage have been included in Fig 10 at the end of the section.

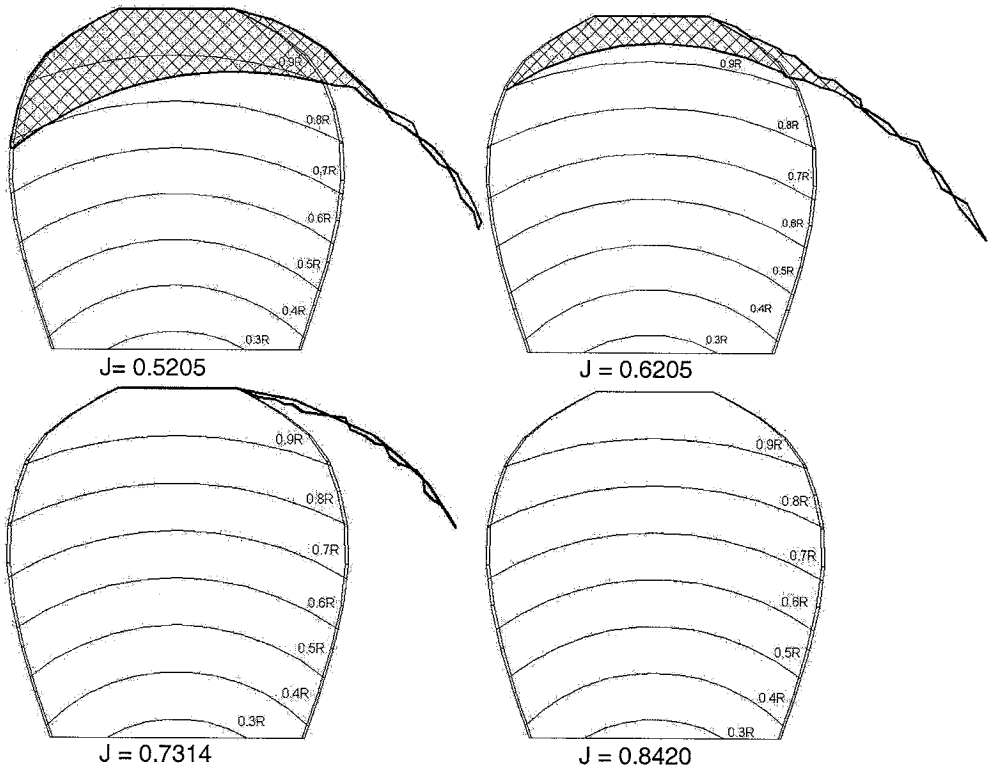

Figure 3.7: Cavitation Diagrams of Blade Suction Side for σ = 2.22

The basic trend toward increasing intensity for decreasing J continued for all cavitation numbers tested. Unfortunately however, as previously mentioned, there was no footage taken of the suction side for any of the higher σ values, only the pressure side. Also, in future testing, it should be noted that cavitation footage be taken for the design conditions. In this instance, that would mean running a full range of J values as close as possible to design sigma of 2.98, and special notice taken around the design J of 0.8. However, this tape still does give us some information about the cavitation activity; we can still see the tip

vortex activity for all the σ values. We can see that all σ values follow similar patterns toward increasing tip vortex intensity with decreasing advance ratios. And correspondingly, also a trend toward a lower advance ratio when this cavitation was first noticed. At advance ratios above 1.05, there is some strange cavitation behavior. This was most common in the lower cavitation values, but still noticeable at J = 1.25 for the highest tested cavitation value of 8.28. It almost resembles cloud cavitation forming in the wake of the propeller. However, it can be contributed to the speed of the water being faster than the speed of advance of the propeller, combined with the higher than normal oxygen content of the water which was over 41% when the tests were carried out. Therefore it is of little concern to the overall cavitation behavior of the propeller. The more important tip vortex cavitation inception points are summarized in the following table, and visualized in the accompanying graph.

σ	$J_{Inception}$
2.15	0.7313
4.20	0.6232
6.16	0.5191
8.20	0.4137

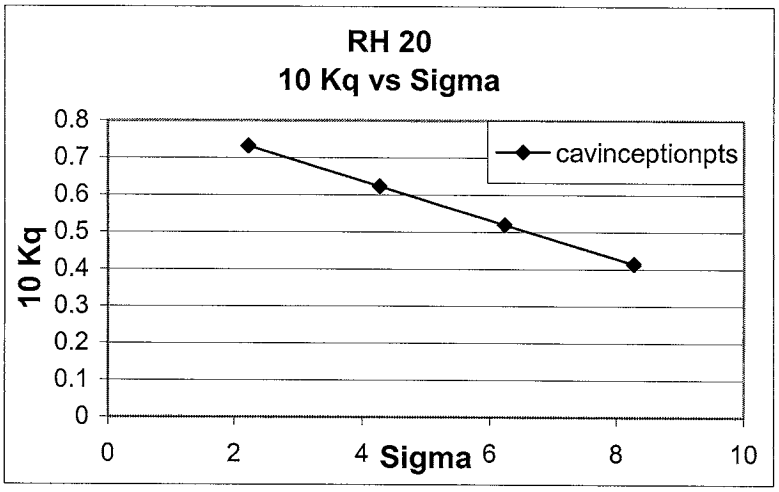

Figure 3.8: Tip Vortex Cavitation Inception Points for Various Sigma

This graph shows an extremely linear relationship, however a more detailed test with smaller divisions in J values would be necessary to gain a fuller understanding of this relationship. However, it is clear that there is a very direct relationship between the cavitation number and the lowest possible advance ratio for cavitation free operation.

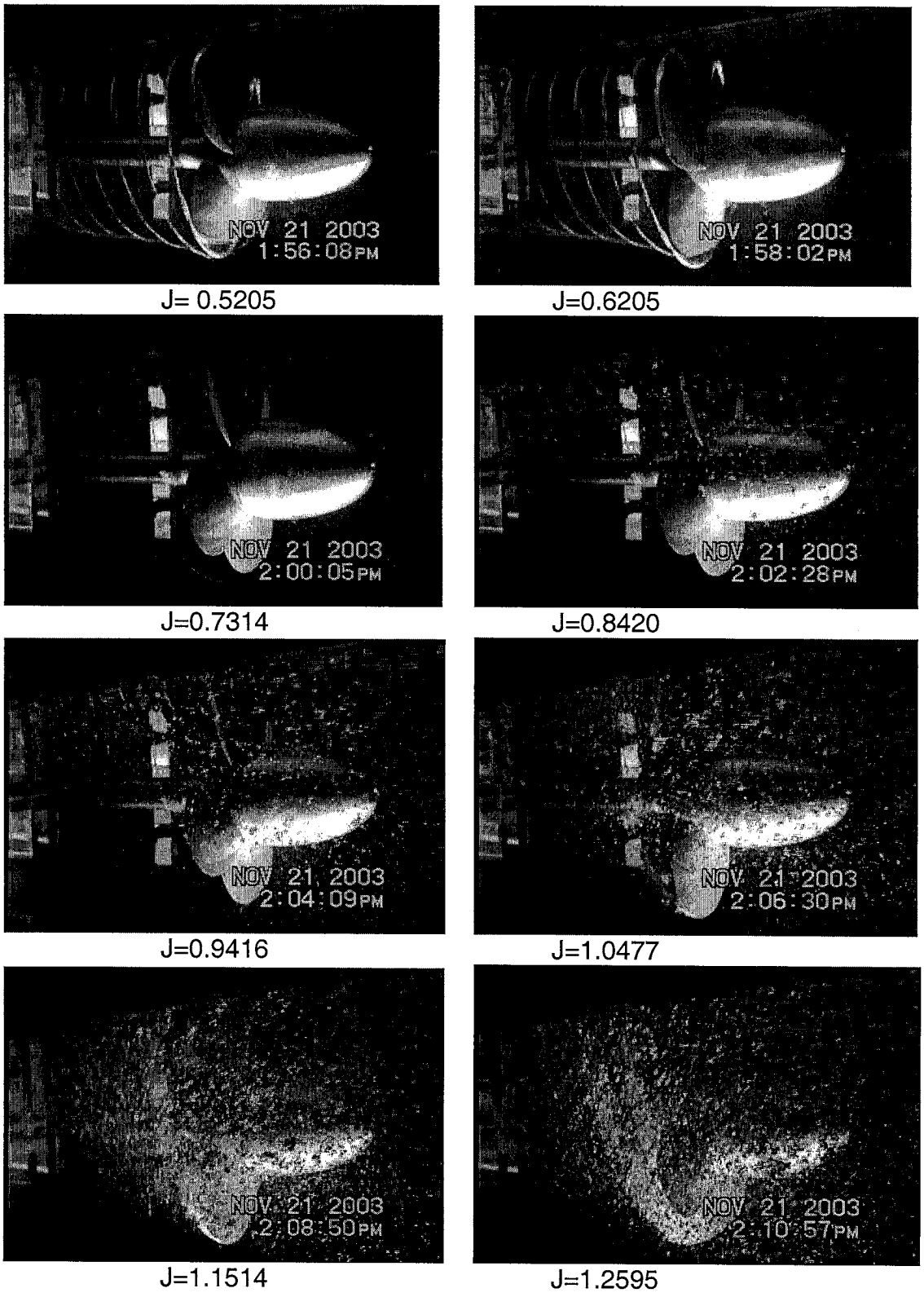

Figure 3.9: Cavitation Results for σ = 2.16

These photos taken directly from the video shot during the cavitation test show all the previously mentioned phenomenon. It is clear to see the bubble cavitation induced by the tank at the higher J values, and the cavitation in the propeller wake at J values above 1.05. But, as previously mentioned, these J represent conditions where the water was moving faster than the propeller.

4.0 SUGGESTIONS FOR FUTURE TESTS

A few suggestions have been made to improve the quality of these tests in the future and they are listed below. In addition to this, there is a copy of the revised test matrix for this test given in Fig. 4.1, as the test will be run again at a later date.

1. Obtain σ = 0.5 or lower. To do this, increase the rotational speed *n* to 30 *rps.*

$$\sigma = \frac{\rho g h + P_{tunnel\_abs} - P_{Vap}}{0.5 \rho n^2 D^2} \tag{3}$$

$$n = \sqrt{\frac{\rho g h + p_{tunnel\_abs} - p_{Vap}}{0.5 \sigma \rho D^2}} = \sqrt{\frac{(1000)(9.81)(0.76) + (10000) - (1230)}{0.5(0.5)(1000)(0.270)^2}} = 29.8\, rps \tag{4}$$

Re-arranging eq.1 to get the above, and the values of 1000 *kg/m*^{3} for ρ, 9.81 *m/s*^{2} for g, 270 *mm* for D, and 10 kPa for p_{tunnel_abs}, which is the minimum attainable tunnel pressure, and 1230 kPa which represents p_{Vap} at 10 °C, will yield a necessary rotational speed of 29.8 *rps.* Therefore using 30 *rps* will allow us to reach the necessary σ. A chart of the temperature and the corresponding vapor pressure is given below in Table 4.1.

Table 4.1: Vapor Pressure of Water for Given Temperatures

Temperature (°C)	Pressure (kPa)
8	1080
10	1230
12	1400
14	1600
16	1810
18	2070

2. At a rotational speed of 30 *rps*, the highest attainable σ value is 6.28; this is shown below in Eq.5, using the maximum attainable tunnel pressure of 200kPa for the value of p_{tunnel_abs} and 30 *rps* for n.

$$\sigma = \frac{\rho g h + P_{tunnel\_abs} - P_{Vap}}{0.5\rho n^2 D^2} = \frac{(1000)(9.81)(0.76) + (200000) - 1230}{0.5(1000)(30)^2(0.27)^2} = 6.28 \qquad (5)$$

If a higher cavitation number is required, then a lower rotational speed must be used.

3. The previous tests lack the data for $\sigma = \sigma_{design} = 2.98$ at $J = J_{design} = 0.8$. This data should be included in future tests, including the performance data and the cavitation video.

4. When the video of the cavitation behavior is being captured, it should be captured from the suction side at all times. The only exception to this is when two cameras are being used, and then one should be placed on the suction side, and the other on the pressure side.

5. Before any testing is done, the propeller should be properly marked. There should be radial positions marked at 0.5R, 0.7R and 0.9R, as well as a mid-chord line to make it easier to assess the severity of the cavitation witnessed.

Cavitation Tunnel Test Matrix for Ducted Tip Propeller Tests PN 42_980_26

Basic Geometry for Propeller PP00+00C0

Pitch ratio at 0.7R	1
Rake	0
Skew	0
Radius	270mm
# of Blades	4

DESIGN SIGMA = 2.9824 --> at 10°C

DESIGN J = 0.8

1.0 Patm=101300 N/m^2

Cavitation number for Sigma = 0.5, 1.0, 2.0, 3.0, 4.0, 6.0

Formula to calculate Tunnel Pressures is as follows;

P_{tunnel_abs} = **0.5 * sigma * rho * n^2 * D^2 - rho * g * h + Pvap**

The following table calculates the required absolute and relative (to atmospheric pressure) tunnel pressure for each cavitation number

Cav. No.	Density (kg/m^3)	Rot. Speed (rps)	Diameter (m)	P_{vapor} (N/m^2)	g (m/sec^2)	Shaft Depth (m)	$P_{tunnel\ abs}$ (N/m^2)	$P_{tunnel\ rel}$ (N/m^2)	P_{atm} ($N/m2^2$)
0.5	1000	30	0.27	1230	9.81	0.76	10176.9	-91123.1	101300
1.0	1000	30	0.27	1230	9.81	0.76	26579.4	-74720.6	101300
1.5	1000	30	0.27	1230	9.81	0.76	42981.9	-58318.1	101300
2.0	1000	30	0.27	1230	9.81	0.76	59384.4	-41915.6	101300
3.0	1000	30	0.27	1230	9.81	0.76	92189.4	-9110.6	101300
4.0	1000	30	0.27	1230	9.81	0.76	124994.4	23694.4	101300
6.0	1000	30	0.27	1230	9.81	0.76	190604.4	89304.4	101300

N = 30 *rps*

J	Va	n	d
0.2	1.62	30	0.27
0.3	2.43	30	0.27
0.4	3.24	30	0.27
0.5	4.05	30	0.27
0.6	4.86	30	0.27
0.7	5.67	30	0.27
0.8	6.48	30	0.27
0.9	7.29	30	0.27
1.0	8.1	30	0.27
1.1	8.91	30	0.27
1.2	9.72	30	0.27

Tunnel Pressure Range is 10 Kpa to 200 Kpa
Max Water Velocity in Test Section is 10 M/s

Figure 4.1: Revised Test Matrix for Model Propeller PP00+00C0

5.0 CONCLUSION

This given propeller hub combination displays good performance properties when the operating conditions require an advance ratio of greater than 0.7313. This was the highest advance ratio when cavitation was first noticed, across the entire range of cavitation values tested. The overall efficiency of the propeller peaked at around J = 0.9, for all sigma values, indicating this is the ideal operating condition for the propeller. As might be expected the propeller generated the most thrust and consequently the most shaft torque at lower advance ratios, as independent of the cavitation condition. The data collected for the higher J values proved to be of little practical use as it indicated thrust generated in the opposite direction to that which was intended. As such these results can be disregarded.

As previously mentioned, the range of tested sigma did not stretch low enough to give a completely rounded view of the performance characteristics of the propeller. As such, any future test should address this issue, either by following the suggestions in section 4, or by some other means. Care should also be taken to ensure that the design σ and the design J are explicitly tested, and that cavitation data is collected for it, as they are the targeted operating conditions for the full-scale propeller being modeled. The tunnel also seemed to produce point anomalies when σ was approximately 4.27. The exact cause of this behavior is unknown. This may be a tunnel power issue, that is the tunnel may just not be able to achieve the necessary conditions, or it may be a calibration issue. Some research has been done into the problem, and it is a consistent error. Which means if it cannot be fixed by recalibration of the tunnel, it can be accounted for mathematically. Whatever the cause, it should be corrected or accounted for before further testing is completed.

Appendix A

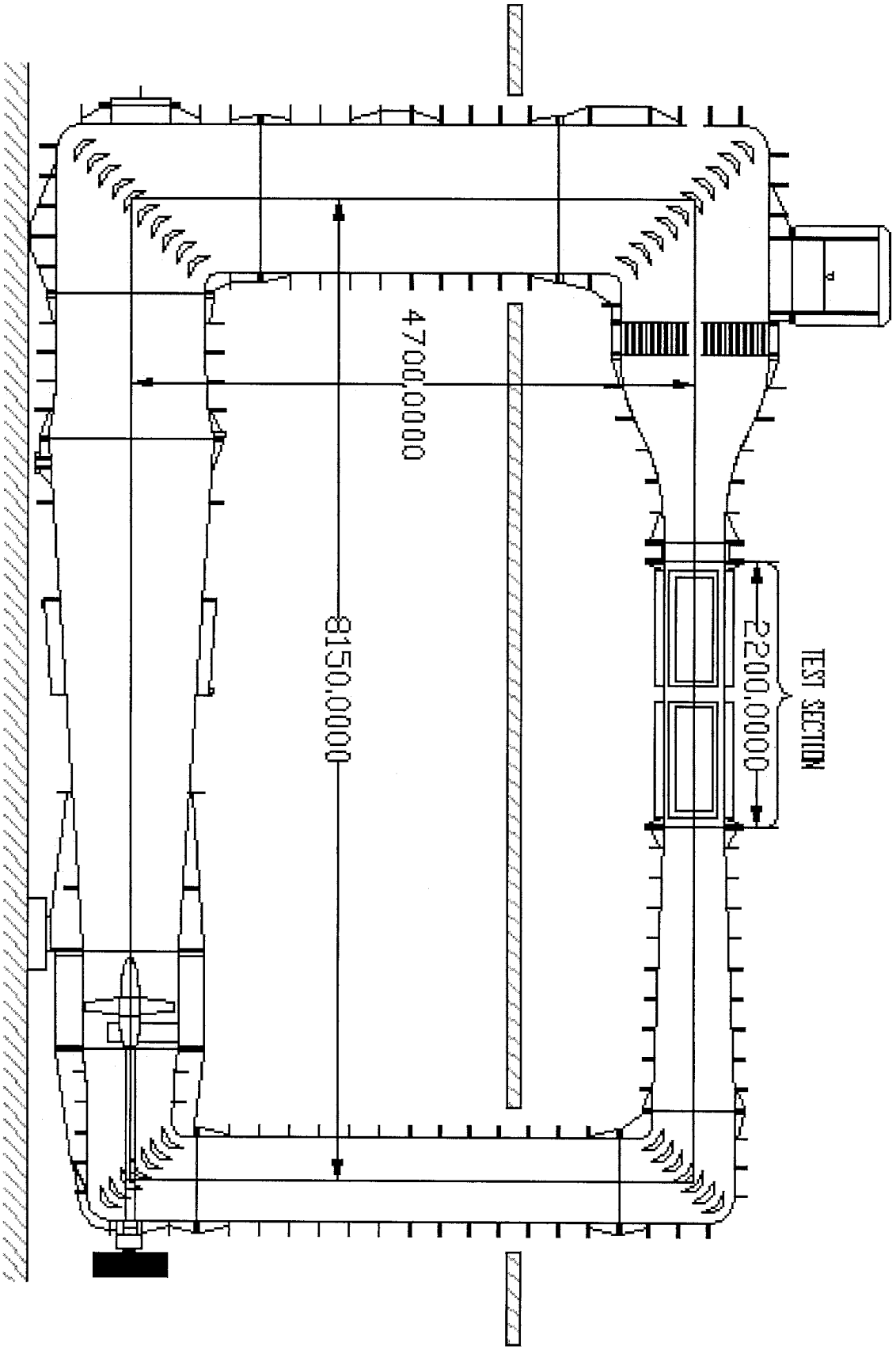
4700.0000
8150.0000
2200.0000
TEST SECTION

REFERENCES

M. Atlar, A.C. Takinaci, E. KorKut, N. Sasaki, T. Aono (2001) "CavitationTunnel Tests For Propeller Noie Of a FRV and Comparisons with Full-Scale Measurements"

M. Doucet (1992) "Cavitation Tunnel Instruction Manual" Report No. OERC92-TR-HYD-92005. Memorial University of Newfoundland.

P. Liu, "Geometrical design of a Podded Propeller Base Model' (Unpublished)

Abbot and A. Von Doenhoff, (1959) "Theory Of Wing Sections". Dover Publications, Inc.

International Towing Tank Conference – Recommended Procedures (2002) "Testing and Extrapolation Methods, Propulsion, Cavitation, Model-Scale Cavitation Tests"

International Towing Tank Conference – Recommended Procedures (2002) "Testing and Extrapolation Methods Propulsion and Cavitation; Description of Cavitation Appearances"